

Supplementary Materials for

Genome-Wide Analysis of a Wnt1-Regulated Transcriptional Network Implicates Neurodegenerative Pathways

Eric M. Wexler,* Ezra Rosen, Daning Lu, Gregory E. Osborn, Elizabeth Martin,
Helen Raybould, Daniel H. Geschwind

*To whom correspondence should be addressed. E-mail: ewexler@ucla.edu

Published 4 October 2011, *Sci. Signal.* **4**, ra65 (2011)
DOI: 10.1126/scisignal.2002282

This PDF file includes:

Methods

References

Fig. S1. Wnt1 differentially modulates Wnt pathway genes across time.

Fig. S2. Wnt1 induces significant early enrichment of genes involved in survival signaling, energy metabolism, and biosynthesis (anabolism).

Fig. S3. Wnt1 induces significant later enrichment of genes involved in blood vessel development, axonogenesis, and Huntington's disease.

Fig. S4. Dynamic time warping (DTW) sensitivity analysis of simulated expression data.

Fig. S5. DTW sensitivity analysis of experimental data.

Fig. S6. DTW identifies Wnt1 effects on cancer-related genes.

Fig. S7. Demonstration of robust blind source separation using parallel independent component analysis (pICA).

Fig. S8. Overview of mutual information-based network inference and sensitivity to thresholding effects.

Fig. S9. Scalable version of Fig. 2: Wnt1 modulates genes implicated in Wnt signaling and Alzheimer's disease (AD).

Fig. S10. Scalable version of Fig. 3: Unsupervised pICA blindly separates gene expression patterns by biological function.

Fig. S11. Scalable version of Fig. 4: Combined topological overlap-based clustering and dynamic Bayesian network construction links Wnt1 signaling with changes in dementia-related genes.

Fig. S12. Scalable version of Fig. 5: Wnt1 induces a gene expression architecture that correlates many well-known dementia genes with Wnt-related signal transduction.

Other Supplementary Material for this manuscript includes the following:
(available at www.sciencesignaling.org/cgi/content/full/4/193/ra65/DC1)

Table S1 (Microsoft Excel format). Overlap of gene changes across time.

Table S2 (Microsoft Excel format). Wnt1-induced immediate changes in known Wnt-related genes.

Table S3 (Microsoft Excel format). Wnt1-mediated enrichment of GO and KEGG pathways varies across epochs.

Table S4 (Microsoft Excel format). Wnt-1 induces changes in genes implicated in AD by genetic association studies.

Table S5 (Microsoft Excel format). GO analysis of whole time series DTW-identified genes.

Table S6 (Microsoft Excel format). Extended ICA gene list and ontology analysis table.

Table S7 (Microsoft Excel format). ICA-GO sensitivity analysis.

Table S8 (Microsoft Excel format). Gene Set Enrichment Analysis of ICA module genes probed against the Broad Institute's Molecular Signatures Database (MSigDB).

Table S9 (Microsoft Excel format). Unique, independent statistical analyses identify similar Wnt1-mediated changes in gene expression.

SUPPLEMENTAL METHODS

Viral Preparation, Infection & Knockdown. Lentivirus was produced by triple transfection of HEK293T cells with plasmids CMVdr8.7 (packaging), pMDG2 (VSV-G envelope), and the viral vector (pLCR-PGRN or pTRIPZ-PGRN), as previously described(1). In both cases, 24-48 hours after transfection, viral supernatants were collected and supplemented with polybrene (4 μ g/ml, Sigma), spun for 3 minutes at 3000 x g, and filtered through 0.45 μ m sterile syringe filter to remove floating 293 cells or debris. Clarified supernatants were concentrated by ultracentrifugation at 50,000g x 90 minutes at 4°C and then re-suspended in Optimem (Invitrogen) supplemented with polybrene (Sigma) 4-8 μ g/ml. Final viral titers $\geq 1 \times 10^8$ /ml were obtained. To fabricate *pLCR*, the internal CMV promoter from pPRIME(232)-CMV-dsRed-FF3(2) was excised and replaced with a promoter that exhibits high levels of transcription and limited repression in hNPs, the CAG fusion promoter from plasmid pLVCT (3). The resulting plasmid pLCR contained the CAG driving the dsRED2 reporter and miR30-based shRNA targeting firefly luciferase, which was used as a negative control (pLCR-FF3). Hairpins against *GRN* were designed cloned into either pLCR or pTRIPZ (Open Biosystems) using the “PCR-shagging” (4) micro-RNA hairpin cloning protocol and then tested for their ability to achieve greater than 50% knockdown of PGRN. Knockdown in TRIPZ-infected cells was induced by addition of doxycycline (2 μ g/ml). APOA4 knockout mice were generated by homologous recombination, and maintained as previously described, prior to harvesting of adult cortical tissues (5, 6).

Immunodetection. Immunoblotting and immunocytochemistry of whole-cell lysates or cultures was performed by standard methods, essentially as previously described (7) (see *Supplemental Methods*) For immunoblotting, rabbit anti-PGRN (Invitrogen) was used 1:500, goat anti-rabbit HRP (Sigma) 1:2000. Mouse anti- β actin (Sigma) was 1:50000, goat anti mouse secondary (Sigma) was 1:5000. For immunocytochemistry, cells were fixed using 4% paraformaldehyde (Sigma). Antibodies used were rabbit anti-activated CASP3 1:1000(Cell Signaling, Danvers, MA), mouse anti-TUJ1 1:1000(Covance, Princeton, NJ) rabbit anti-GFAP 1:2000(Sigma), Alexa donkey anti-rabbit 488 1:1000(Invitrogen), Alexa

donkey anti-mouse 488 1:1000(Invitrogen), and Alexa goat anti-rabbit 647 1:1000(Invitrogen). Cells were counterstained with DAPI and 6 high-power fields were counted per coverslip.

Reporter assays: For GRN reporter assays 293T cells (ATCC) were transfected with 50 ng of reporter construct expressing *Photinus pyralis* (firefly) luciferase, 1 ng of Renilla luciferase plasmid (pRL-EF), and 50 ng of pCMV-Tag4a PGRN expression plasmid (Switchgear Genomics, Menlo park CA) using FuGENE (Roche Applied Science) according to the manufacturer's instructions. Forty-eight hours later, cells were lysed and analyzed using the dual luciferase reporter assay system (Promega) according to the manufacturer's instructions and luminescence was read on a Synergy-2 Plate reader (Biotek). Co-transfection of Renilla was used for transfection normalization, and values were additionally normalized to cells transfected with a promoter-less luciferase construct. For canonical Wnt reporter assay hNPS were infected with a lentivirus containing an enhanced TOP promoter (OTP) driving destabilized GFP (dsGFP) (8, 9), or a similar promoter driving luciferase. The latter contains an SV40 promoter constitutively driving red fluorescent protein (RFP), thereby allowing internal normalization and the selection of stable reporter cells (10). Luminescence or fluorescence was quantified as above or as previously described (1).

SUPPLEMENTAL REFERENCES

1. Wexler, E. M., A. Paucer, H. I. Kornblum, T. D. Palmer, and D. H. Geschwind. 2009. Endogenous Wnt signaling maintains neural progenitor cell potency. *Stem Cells* 27:1130-1141.
2. Stegmeier, F., G. Hu, R. J. Rickles, G. J. Hannon, and S. J. Elledge. 2005. A lentiviral microRNA-based system for single-copy polymerase II-regulated RNA interference in mammalian cells. *Proc Natl Acad Sci U S A* 102:13212-13217.
3. Szulc, J., M. Wiznerowicz, M. O. Sauvain, D. Trono, and P. Aebischer. 2006. A versatile tool for conditional gene expression and knockdown. *Nat Methods* 3:109-116.
4. Paddison, P. J., A. A. Caudy, E. Bernstein, G. J. Hannon, and D. S. Conklin. 2002. Short hairpin RNAs (shRNAs) induce sequence-specific silencing in mammalian cells. *Genes Dev* 16:948-958.
5. Weinstock, P. H., C. L. Bisgaier, T. Hayek, K. Aalto-Setälä, E. Sehayek, L. Wu, P. Sheffele, M. Merkel, A. D. Essenburg, and J. L. Breslow. 1997. Decreased HDL cholesterol levels

but normal lipid absorption, growth, and feeding behavior in apolipoprotein A-IV knockout mice. *J Lipid Res* 38:1782-1794.

6. Whited, K. L., D. Lu, P. Tso, K. C. Kent Lloyd, and H. E. Raybould. 2005. Apolipoprotein A-IV is involved in detection of lipid in the rat intestine. *J Physiol* 569:949-958.
7. Nakano, I., K. Joshi, K. Visnyei, B. Hu, M. Watanabe, D. Lam, E. Wexler, K. Saigusa, Y. Nakamura, D. R. Laks, P. S. Mischel, M. Viapiano, and H. I. Kornblum. 2011. Siomycin A targets brain tumor stem cells partially through a MELK-mediated pathway. *Neuro Oncol* 13:622-634.
8. Yu, X., and R. C. Malenka. 2003. Beta-catenin is critical for dendritic morphogenesis. *Nat. Neurosci.* 6:1169.
9. Reya, T., A. W. Duncan, L. Ailles, J. Domen, D. C. Scherer, K. Willert, L. Hintz, R. Nusse, and I. L. Weissman. 2003. A role for Wnt signalling in self-renewal of haematopoietic stem cells. *Nature* 423:409.
10. Fuerer, C., and R. Nusse. 2010. Lentiviral vectors to probe and manipulate the Wnt signaling pathway. *PLoS ONE* 5:e9370.

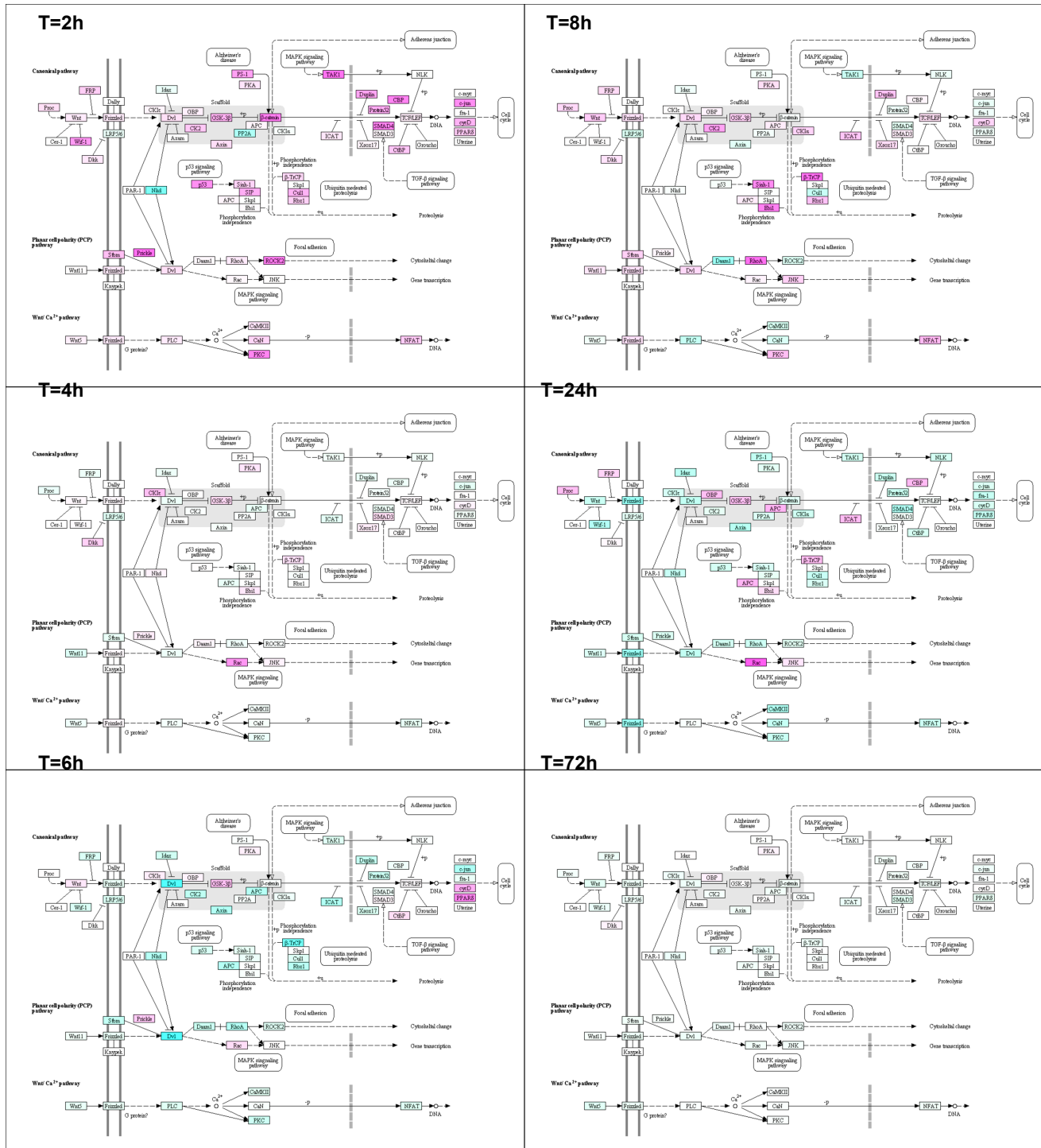
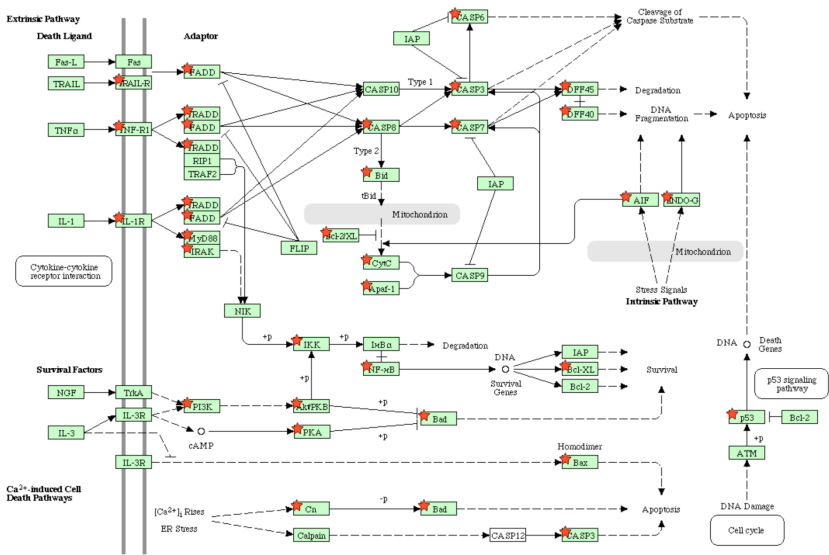
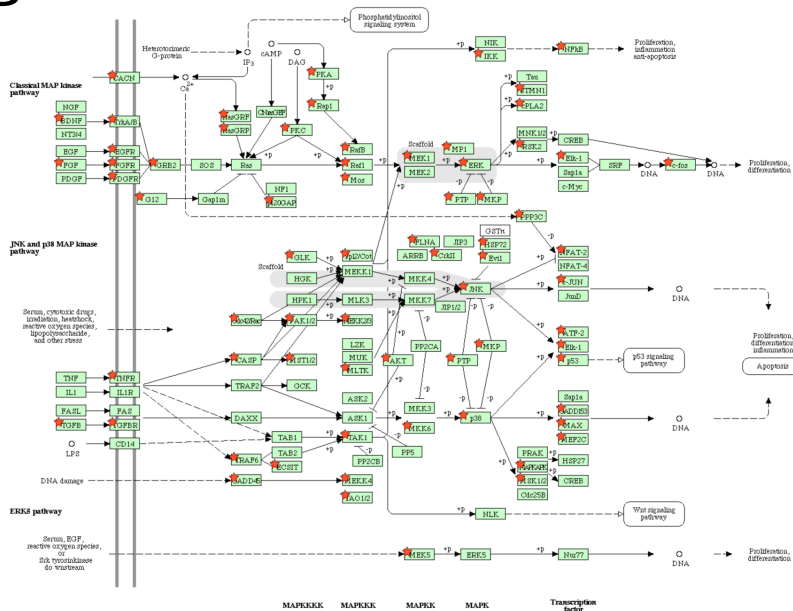


Figure S1. Wnt1 differentially modulates Wnt pathway genes across time. Wnt1 changes expression of genes in both canonical and non-canonical pathways. Color saturation is proportional to p-value (Magenta: Upregulated, Cyan: Downregulated).

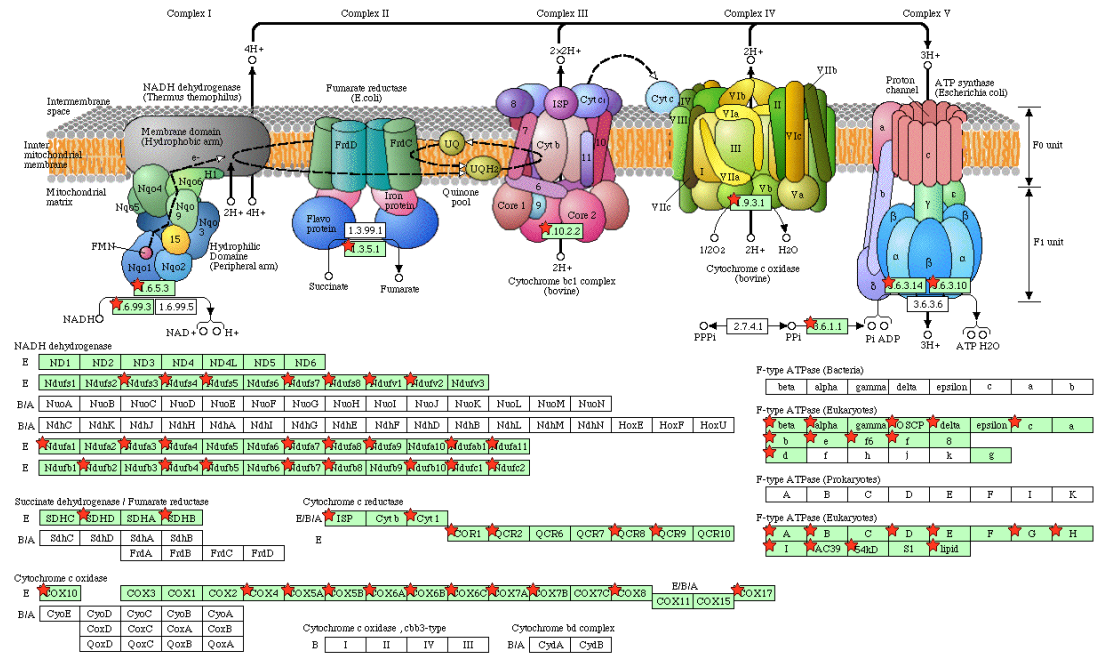
A



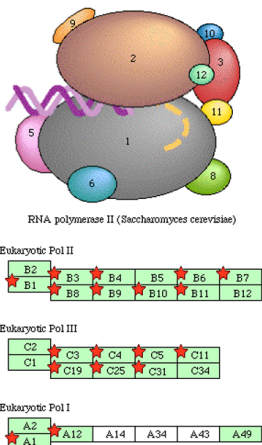
B



C



D



E

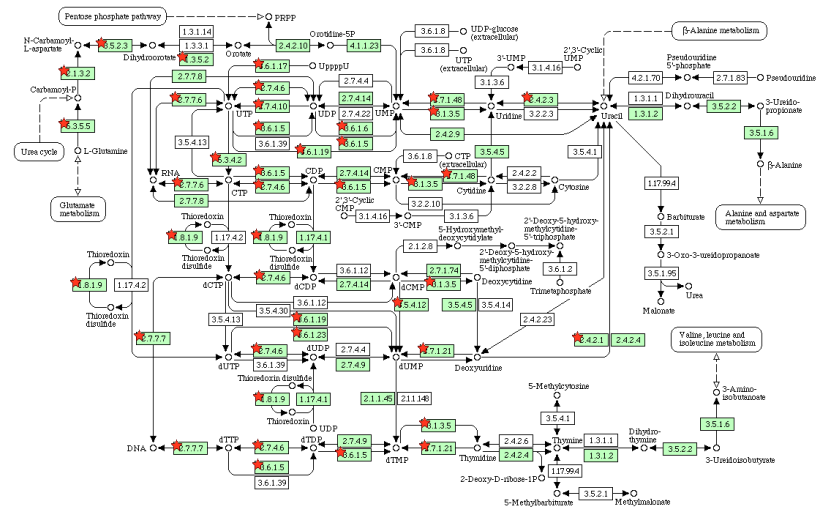


Fig. S2. Wnt1 induces significant early enrichment of genes involved in survival signaling, energy metabolism, and biosynthesis (anabolism). DAVID-identified KEGG pathways: (A) Apoptosis and (B) MAP Kinase signaling & survival significantly enriched at 2 hours after Wnt1 application. (C) KEGG pathway: Oxidative Phosphorylation significantly enriched at 2 hours after Wnt1 application. (D) KEGG pathways (A) RNA polymerase (B) pyrimidine metabolism significantly enriched at 6 hours after Wnt1 application. Significantly enriched KEGG pathways (FDR≤5%) Stars indicate significantly changed genes (DAVID modified Fisher exact test; p≤0.05).

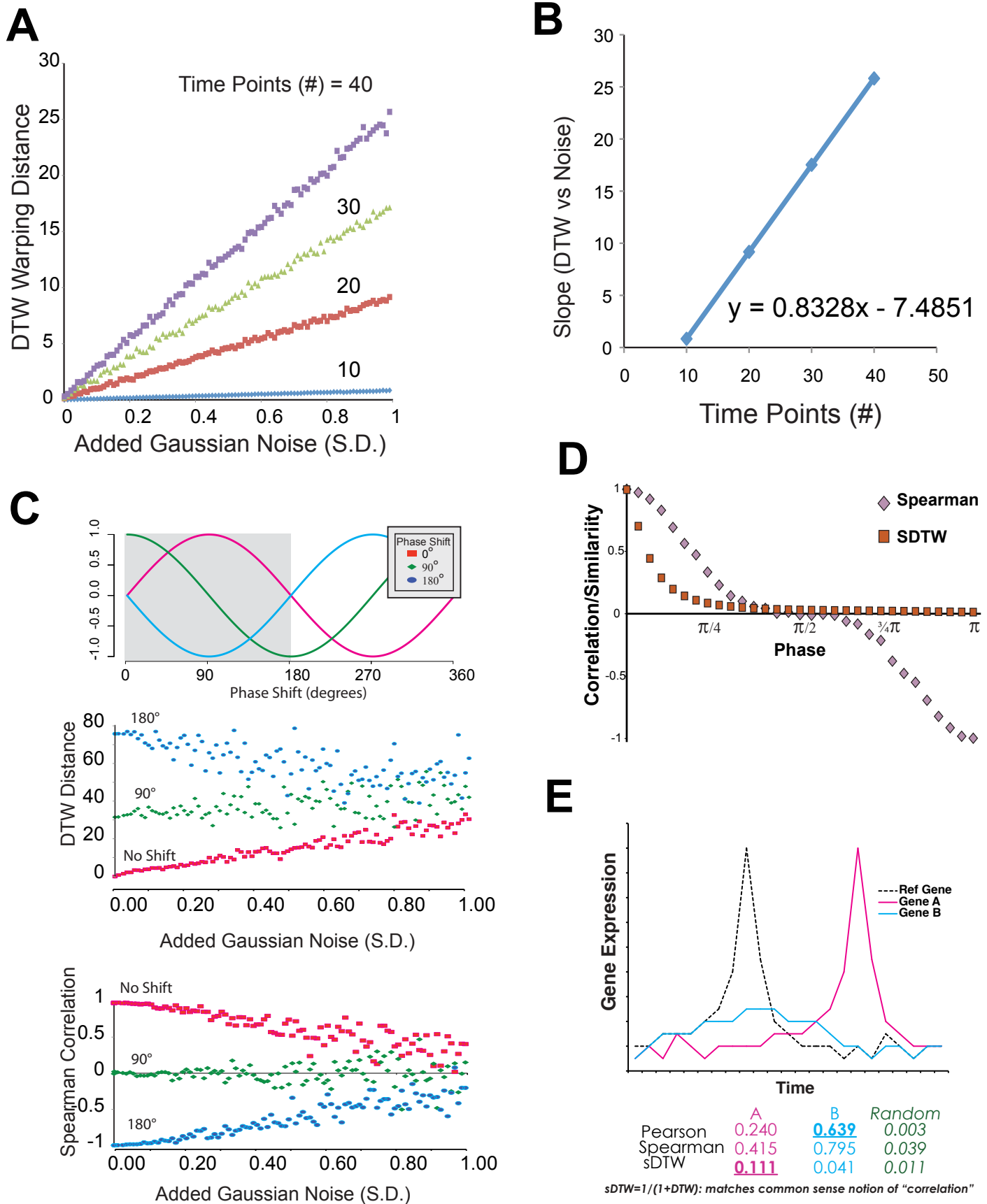


Fig. S4. Dynamic Time Warping sensitivity analysis of simulated expression data (A-B) DTW between random traces: (A) Illustration of the linear relation between the DTW distance and the amount of noise present; the slope of this relation is linearly proportional to the number of time points (B). (C-D) Effects of phase shifting on DTW distance. (C) Gene expression was initially modeled as a set of sine waves phase-shifted by 90 (Green) or 180 degrees (Cyan) from the reference (Magenta) trace. These traces were then mixed with increasing amounts of Gaussian random noise; then DTWdist was computed between the reference and phase- shifted noisy trace and plotted (Upper). Spearman rank correlation was computed for the same traces (Lower) (D) DTW distance vs. Spearman correlation of identical phase shifted time courses. To facilitate comparison, DTWsimilarity (sDTW) was plotted against the Spearman coefficient for the phase-shifted traces. (E) DTW is superior to Correlation for analysis of phase-shifted expression transients. sDTW, Pearson, and Spearman correlations were calculated between the expression of the reference gene (black dotted line) and either a nearly- identical, phased variant (Gene A; Magenta) or another that exhibits minimal time-dependent changes in expression (Gene B, Cyan).

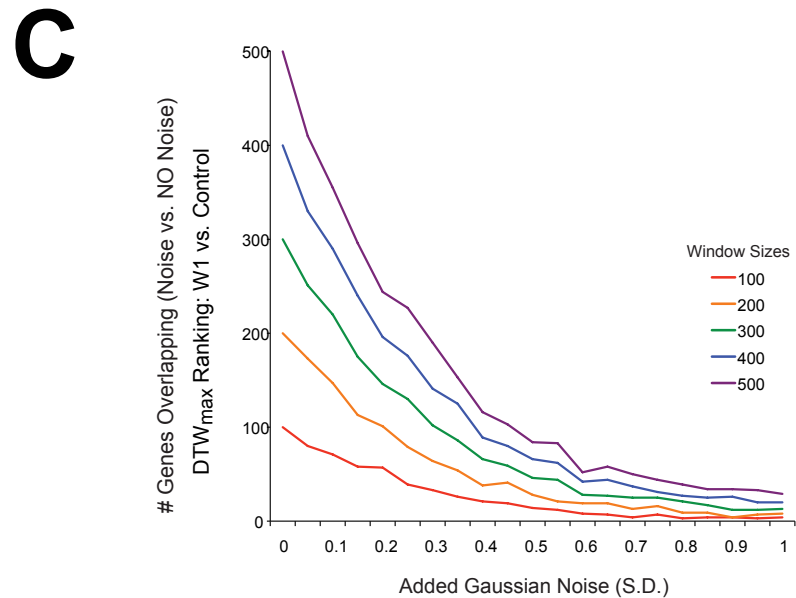
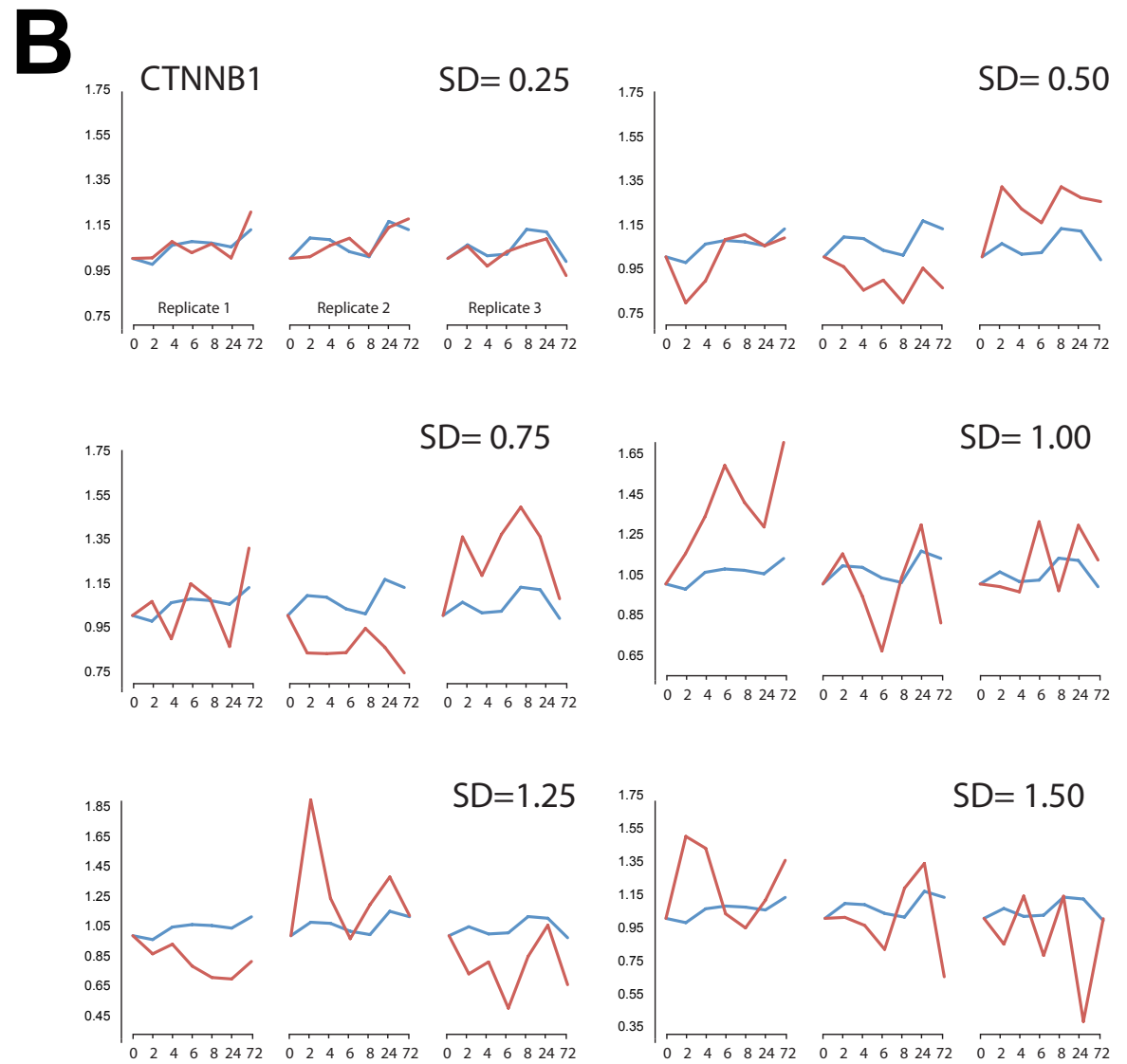
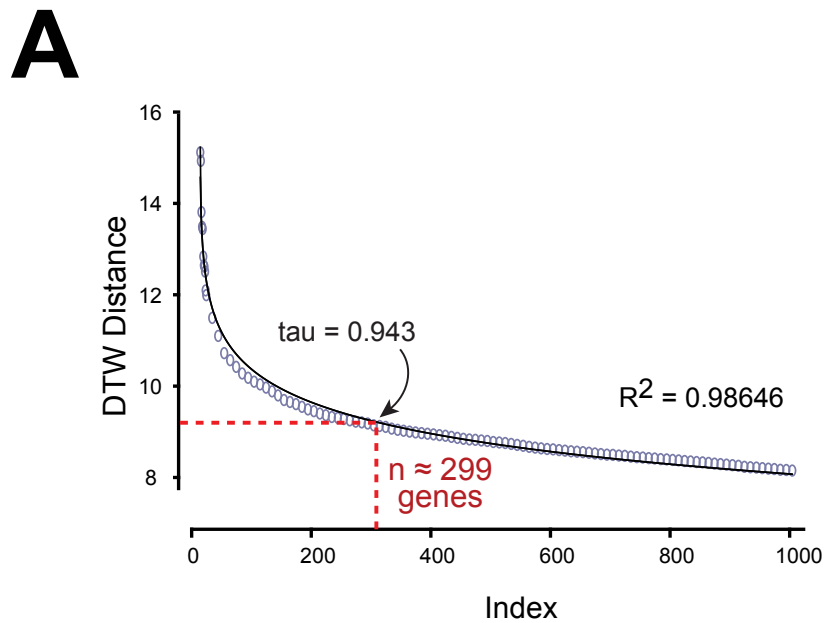


Fig. S5. Dynamic Time Warping sensitivity analysis of experimental data (A) Distribution of DTW distances. Plotted are the ranked DTW distances (Wnt1 treated vs. control) for the top 1000 genes, showing an exponential rate of decline ($\tau = 0.94$, $R^2 = 0.99$), where one decay constant (τ) corresponds to the 299th gene. (B) The effects of adding increasing amounts of noise (red traces) with measured expression (blue) of the gene β -catenin (CTNNB1). This confirms that the ability to resolve similarities between lists ranked by DTWdist, as measured by overlap, declines steadily with a predictable exponential decay (i.e. no sharp fall-off). (C) Effects of noise on DTW-based gene ranking. For each gene, DTWdist was calculated between time-series, for Wnt1-treated or untreated (control) hNPs, then ranked in descending order (i.e. the largest DTW distance corresponds to the most specific effect of Wnt1 treatment). Plotted are the numbers of genes overlapping between the ranked list of DTW measurements in the absence or the presence of added noise. The individual curves represent the overlap when calculated for different window sizes (i.e. number of genes compared for overlap). As shown, 0.25 S.D. of added noise consistently reduces the DTW by 50%, across window sizes.

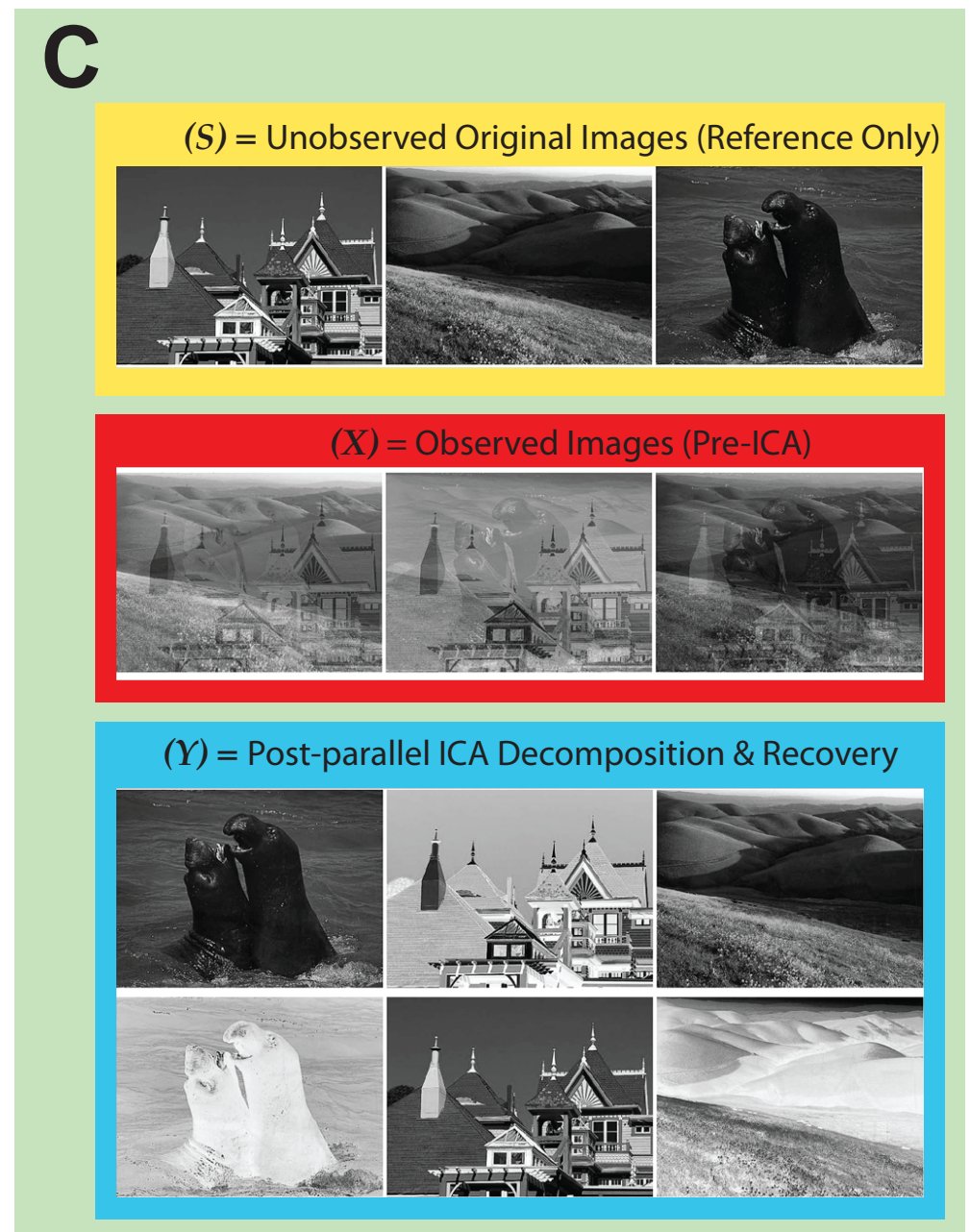
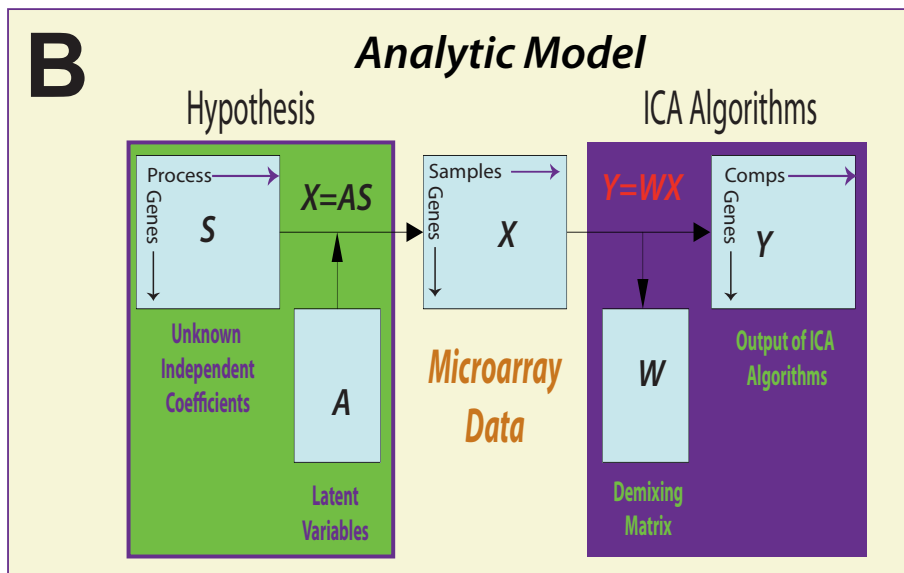
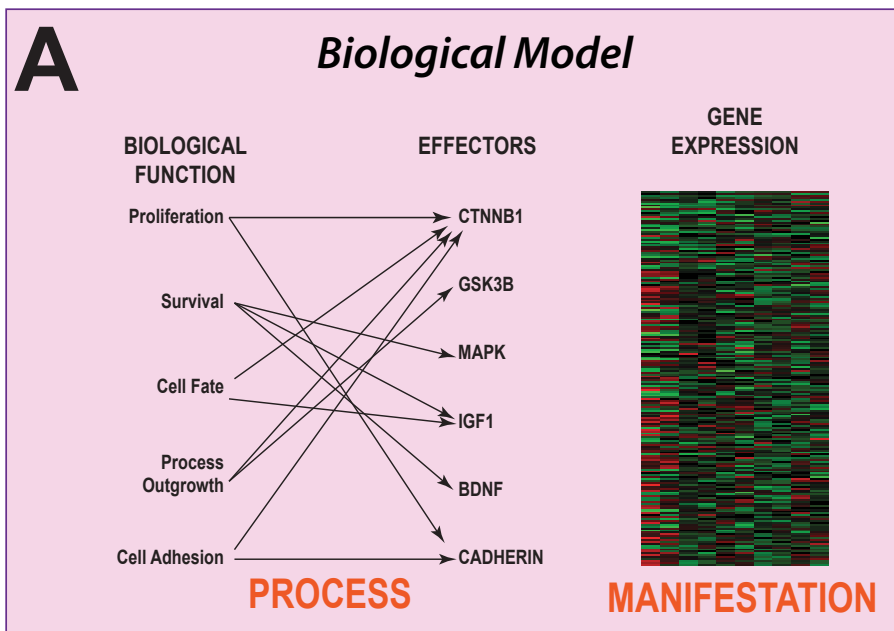


Fig. S7. Demonstration of robust blind source separation using parallel independent component analysis. (A) An illustration of the biological mixing model. In this example, many genes subserve a single biological process and in turn, each gene is involved in one or more biological processes. As such, the observed expression for each gene is the sum of its contribution to each process, creating a matrix of Genes x Biological Processes and (B) Analytic model that underlies the use of pICA. Expression data are cast as a matrix of Genes x Samples (arrays). Application of pICA to these data will unmix the latent variable (biological processes). In practice, these "recovered" biological processes may be a single process. More commonly it is a metaprocess that comprises several coordinated cellular processes (e.g. synapse formation and transmitter vesicle synthesis). (C) Visual demonstration of blind source separation using fastICA. The three reference images (top; highlighted in yellow) were randomly mixed to create the "observed" images (middle; highlighted in red). These are analogous to experimentally-obtained microarray data, whereas the reference images can be thought of as the underlying biological processes. We applied the fastICA algorithm, exactly as we applied it to our data in Fig. 3, to decompose these images into parallel independent components (bottom; highlighted in blue). Because the algorithm is insensitive to sign, both the positive and negative component images are displayed. As shown, this approach recovers the original images with high fidelity, even with no prior knowledge of their content.

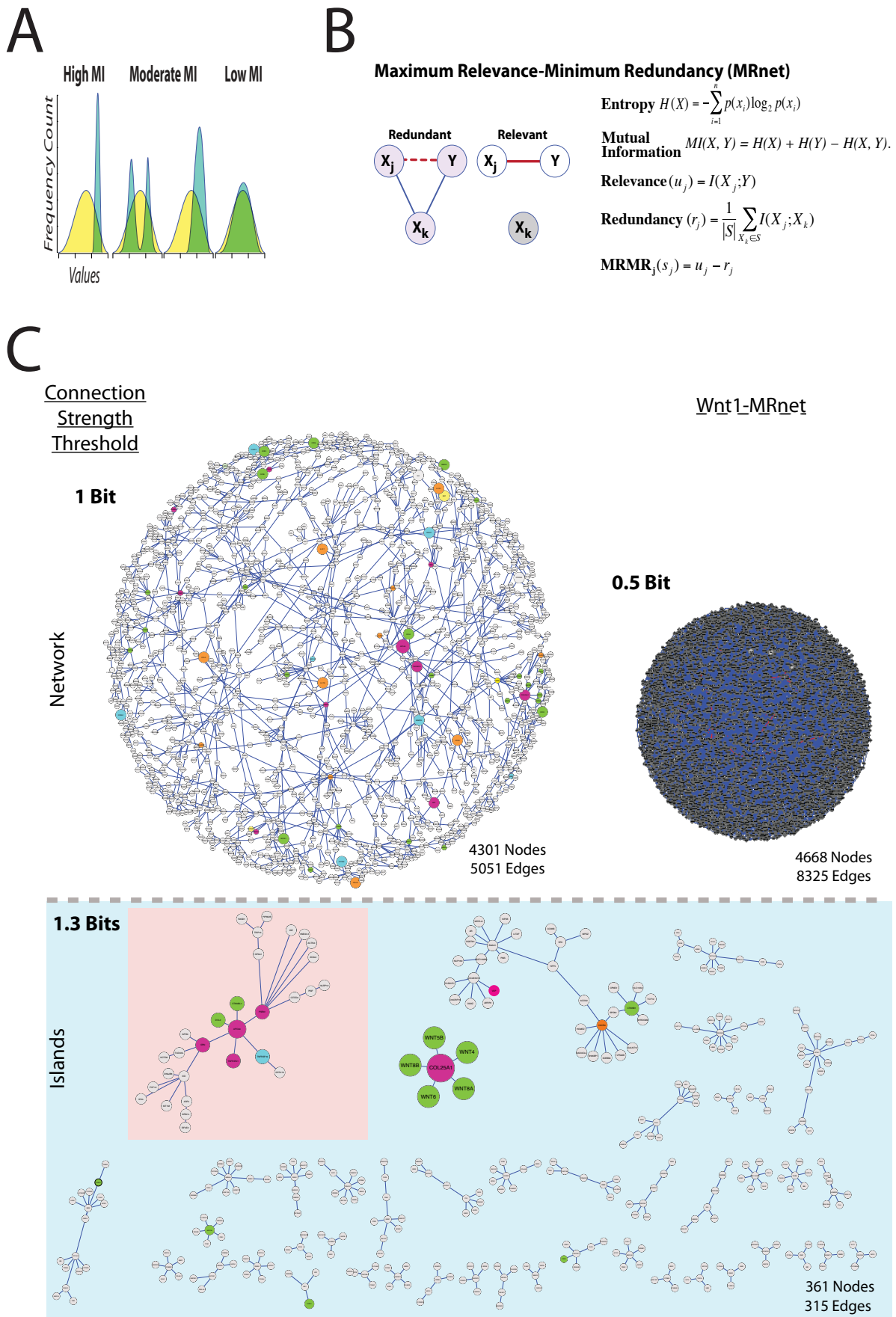
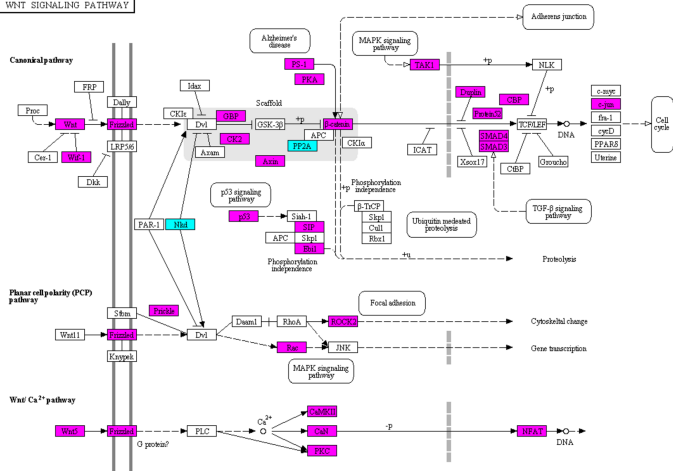


Fig. S 8. Overview of mutual information-based network inference and sensitivity to thresholding effects. (A) Graphical representation of the operational definition of Mutual Information (MI), whereby the information shared between two variables X (Blue) and Y (Yellow) is the amount of uncertainty about X that is reduced by knowing Y. As depicted, knowing the distribution of Y confines the possible values of X to lie within the overlap of the distributions (the region in green). (B) Summary of the equations used to calculate the discrete information theoretic quantities (Entropy, Mutual Information, Relevance and Redundancy) used to build and prune our maximum relevance-minimum redundancy coexpression network. (C) Network architecture: Use of increasingly stringent edge weighting criteria (i.e. higher MI) causes a loss of network cohesion while preserving a power law distribution of connectivity among gene islands. Dementia related genes (Magenta). Wnt related genes (Green).

A

WNT SIGNALING PATHWAY



B

ALZHEIMER'S DISEASE

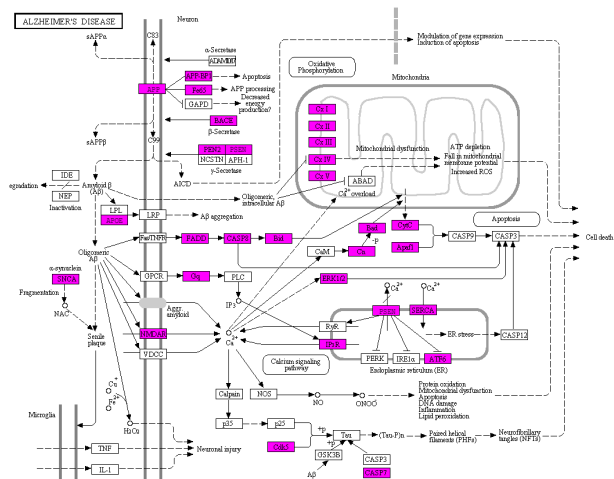


Fig. S9. (Scalable version of Fig. 2) Wnt1 modulates genes implicated in Wnt signaling and Alzheimer's Disease. (A) KEGG pathway: Graphical summary of the diversity of Wnt signaling-related genes (canonical and non-canonical), significantly enriched (FDR≤5%) at 2 hours after Wnt1 application (n=59 out of 151 KEGG Wnt genes). Significantly increased (Magenta) or decreased (Cyan) mRNA abundance (t-test *p≤0.05) (B) KEGG Alzheimer's Disease pathways highlighting genes (Magenta) whose message was significantly increased by Wnt1 at (a) t=2 hours and (t-test *p≤0.05).

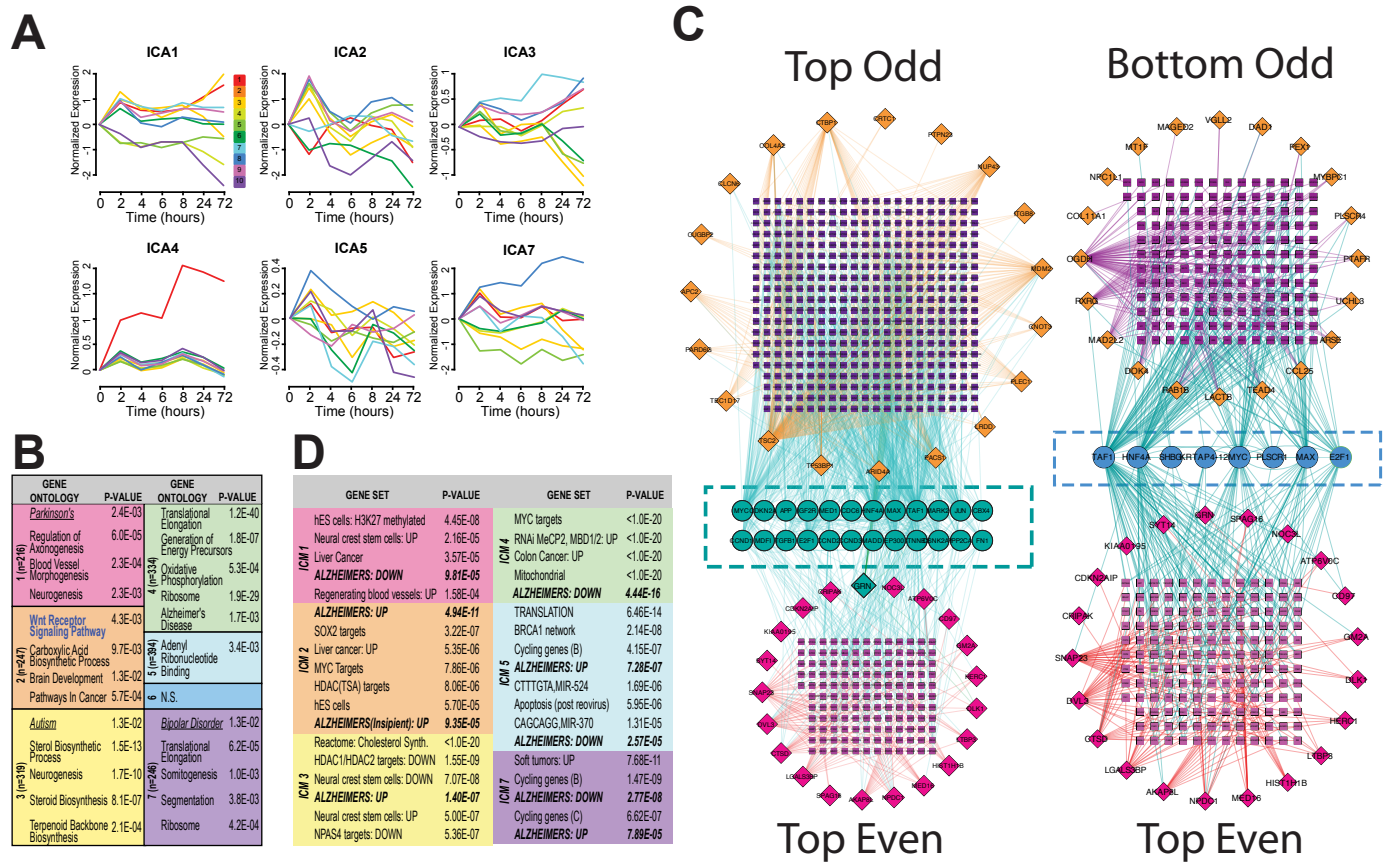


FIG. S10. (Scalable version of Fig. 3) Unsupervised Parallel Independent Component Analysis (pICA) blindly separates gene expression patterns by biological function. (A) Normalized, mean expression time course for the top ten genes in each ICA component, ranked by gene loading. (B) GO enrichment via DAVID was performed on each independent component module, following thresholding at a gene-loading level of 3.0. Colors delineate individual modules. Listed are the top non-redundant level-5 biological processes (129), Disease ontologies (underlined) or KEGG pathways (boldface), with associated p-values (n.s. none significant, n= number of genes per module). (C) Overlapping MiME interactome networks built using the top 20 odd ranked genes versus top 20 even ranked genes from ICM2 (Left: Top Odd vs Top Even), or (Right: Bottom vs Top) networks built from the bottom 20 genes versus Top Even genes. The Top-Odd network recovered significantly more Top-even genes (Green Circles; n=24) than did the Bottom network (Blue Circles; n=8). (D) Genes in each ICM were probed against the Broad Molecular Signature database. The most highly enriched dataset is presented for each module, as well as a representative sampling of other significantly enriched data sets.

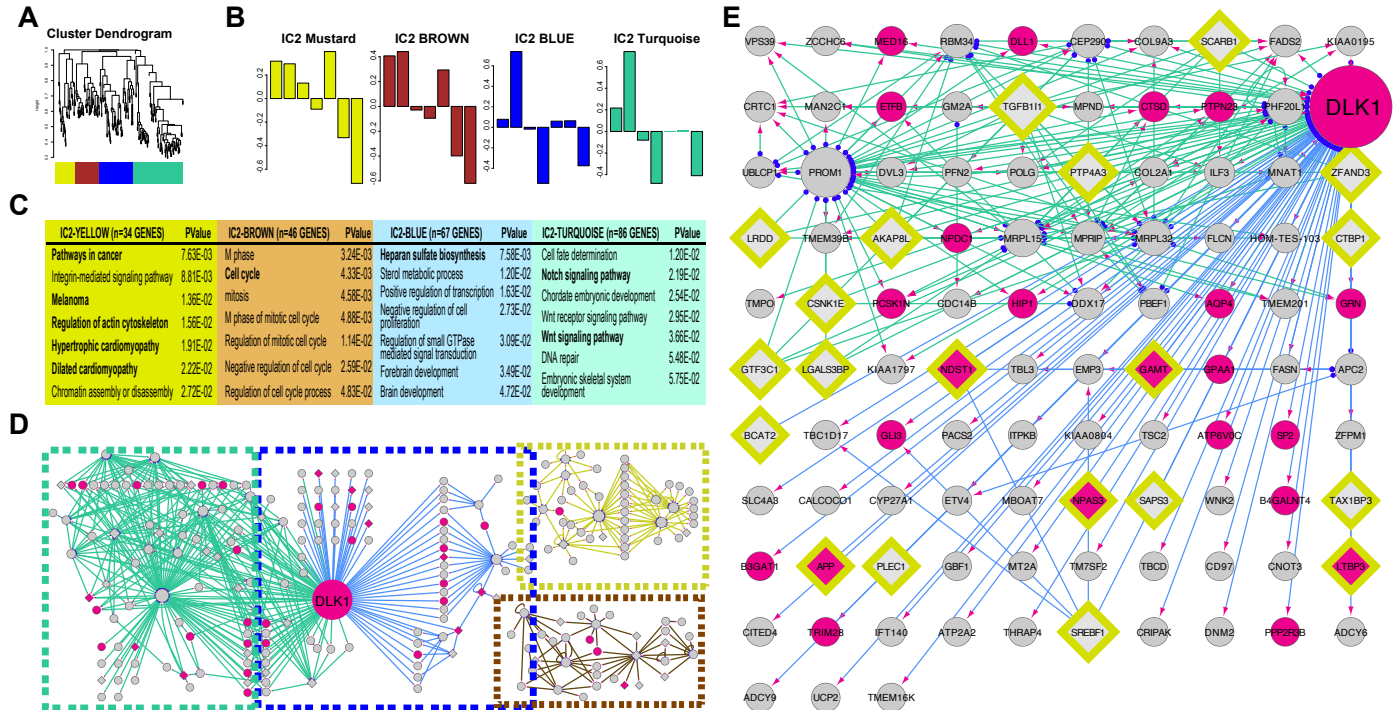


Fig. S11. (Scalable version of Fig. 4) Combined topological overlap-based clustering and dynamic Bayesian network construction links Wnt1 signaling with changes in dementia-related genes. (A-B) WGCNA clustering of ICM2 genes: Wnt1-stimulated expression time-courses for the genes comprising the ICM2 module were averaged, then subjected to TOM-WGCNA based clustering (A). This produced four submodules (Mustard, Brown, Blue and Turquoise). (B) Submodule eigengenes, where singular value decomposition was used to extract a characteristic first principle component eigengene for each submodule. Y-axis is eigengene expression. (C) GO analysis reveals functional uniqueness of individual submodules. (D-E) Dynamic Bayesian Network (DBN) depicting causal relationships, within each module. (D) Overview of the DBN network: Edge-color codes the original submodule. Node color indicates those genes identified by DTW analysis (Red; n=23). Outlined Diamonds denote those genes whose expression was increased in the brains of Alzheimer's patients (n=20) (70). Delta-like 1 homolog (DLK1) forms the primary hub in this network. [Note: SORT1 (sortilin-1), like DLK1, is a binding partner for progranulin (73).] (E) A more detailed view of the DLK1 hub and its associated genes, revealing a significant overlap (hypergeometric $p \leq 0.001$) with DTW identified genes and a strong enrichment for genes with increased message in

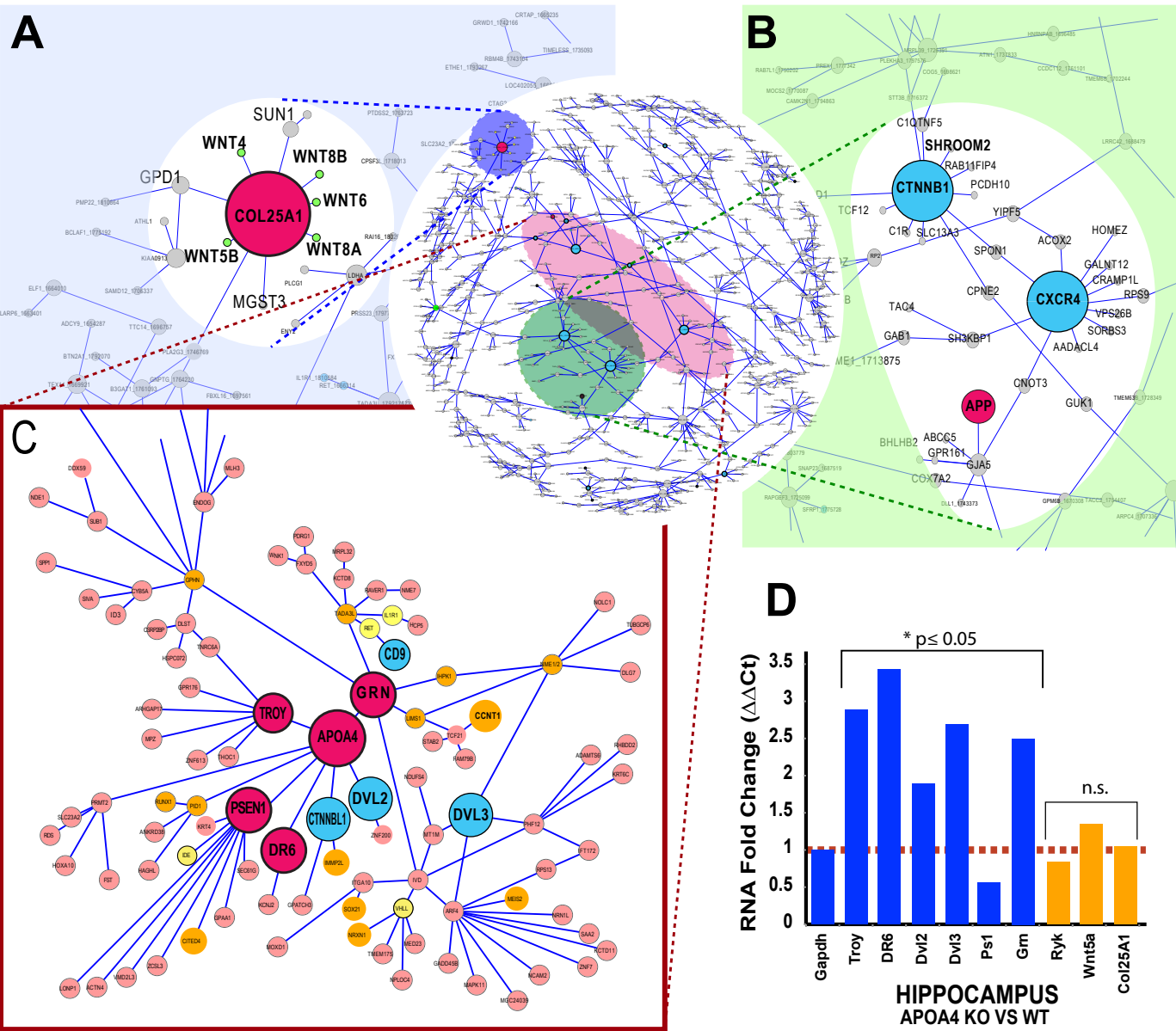


Fig. S12. (Scalable version of Fig. 5) Wnt1 induces a gene expression architecture that correlates many well-known dementia genes with Wnt-related signal transduction. (A-C) Microarray-based gene expression data was generated from Wnt1- treated or untreated hNPs, followed at 7 seven time-points over 72 hours and repeated in triplicate. Displayed is the subset of the MINA-based network thresholded at 1.1 bits. (A) Multiple Wnt5 cluster around COL25A1, an AD-related gene. (B) CTNNB1 (β -catenin) and CXCR4 hubs. (C) Neighborhood containing a dense cluster of dementia [Magenta; presenilin (PSEN1), progranulin (GRN), APOA4, DR6 (Death Receptor-6)] and Wnt transduction related genes. Nodes are color coded to reflect genes implicated in neural development (Orange), dementia (Magenta), Wnt signaling (Cyan), or diseases distinct from dementia (Yellow). [Note: CCNT1 (cyclin-T1) is a binding partner of PGRN] (D) Loss of APOA4 dysregulates dementia hub genes: qPCR of hippocampal gene expression among wild type and APOA4 null mice reveals significant changes in the expression of connected genes (Blue), relative to GAPDH, but not the other Wnt-dementia hub gene COL25A1 (Orange). Values are fold changes in gene expression calculated using delta-delta Ct method (* $p \leq 0.05$; $n = 4$, PCR-ANCOVA).